SEMI-ACTIVE CONTROL OF FRICTION DAMPERS

P. Dupont, P. Kasturi and A. Stokes

Aerospace & Mechanical Engineering, Boston University, Boston, MA 02215, U.S.A.

Semi-active control of friction dampers has been proposed to improve the energy dissipation characteristics of passive friction dampers and to broaden the areas of application in which they can successfully be used. In this paper, we propose control laws for friction dampers which maximize energy dissipation in an instantaneous sense by modulating the normal force at the friction interface. In particular, we consider the effect of displacement- and velocity-induced friction dynamics on the design of the control law. A dynamic controller is proposed that prevents stored frictional energy from being returned to the system. Using both simulation and experimental results, we demonstrate under what operating conditions friction dynamics are vital to the control problem and, for these conditions, demonstrate the efficacy of the proposed controller. Furthermore, the experiments reveal that control strategies which, unlike instantaneous optimization, take system dynamics into account could lead to significant additional improvements in energy dissipation.

© 1997 Academic Press Limited

1. INTRODUCTION

Friction dampers have been proposed for use in a broad variety of applications. For example, passive friction dampers are currently used in the turbines of aircraft engines as well as power plants (see, e.g., reference [1]). They may be designed to limit maximum blade strain during operation near resonance or they may be employed to mitigate flutter. In the latter case, the control objective is to maximize energy dissipation.

As a second example, note that one of the major sources of energy dissipation in large space structures is the joints and fittings. Energy dissipation takes place in the joints due to very small amplitude oscillatory motion at the friction interfaces. The frequency of oscillations in these structures is usually in the range of 0·1–5 Hz, depending upon the size and stiffness of the structure [2, 3]. Friction dampers are proposed, for these applications, to enhance energy dissipation.

In most cases, friction dampers have been studied in a passive context (see, e.g., reference [4]). Damping performance may be greatly improved, however, with only a modicum of expense, by controlling the normal force applied at the friction damper. This notion of producing a damping force by controlling a secondary variable, termed semi-active control, is apparently attributable to Karnopp and co-workers, who first proposed varying the force of a viscous damper by controlling its orifice area [5]. The appeal of semi-active control is that performance levels rivalling fully active control can be achieved with a fraction of the input power required of active control. The application of semi-active control to friction dampers was first proposed by Ferri and co-workers [6]. Semi-active control has been applied to other types of dampers; e.g., dampers made with electro-rheological fluids [7, 8].

The control objective of this paper is to maximize energy dissipation in an instantaneous and local sense. This approach is taken because improved damping is the most common motivation for considering friction dampers. Furthermore, controlled friction dampers which use only local, instantaneous information possess advantages in terms of cost, ease of implementation and, in the case of systems with multiple dampers, tolerance of partial failure. A limitation of instantaneous maximization is that a constraint on rattle space, the maximum stroke of the damper, cannot be explicitly included in the design process.

It should be noted that, according to the task at hand, alternate objectives involving the minimization of structural strain or peak accelerations could be more germane than energy dissipation. To our knowledge, these approaches have been pursued in only a few cases [6].

1.1. CONTROL OF SEMI-ACTIVE DAMPERS

Several approaches have been taken to derive semi-active control laws which maximize damper energy dissipation. The first is to write the Lyapunov function representing system energy. By inspection of its time derivative, one may arrive at a bang–bang control law that maximizes the damping contribution of the controlled term. This approach was applied to electro-rheological fluid dampers in references [7, 9]. Although unstated, the fluid model employed is equivalent to Coulomb plus viscous friction.

A second approach employs LQR theory [6]. The cost function is an infinite time integral of a weighted sum of system energy and control effort. Ferri and co-workers have compared controllers in which the input is constrained during and after the optimization. In the latter case, the controller may call for negative normal forces. An *ad hoc* modification of this controller to force $F_N \geqslant 0$ is called Clipped LQR Control. Both the optimal and clipped controllers are shown by simulation to perform favorably in comparison to a control law in which $F_N = k|v|$, where v is the relative sliding velocity at the damper and $k > 0$ is constant. This velocity proportional controller does, however, prevent the damper from sticking. Note that a sticking damper does not dissipate energy.

Sliding mode control of an electro-rheological fluid damper has also been investigated [8]. In this case, the fluid is modelled with a viscous component related linearly to the applied electric field and a Coulomb component related quadratically to the electric field. A first order sliding surface is defined for each damper and a bang–bang control law is developed which maximizes the rate at which each damper approaches its sliding surface. Since the only point on the sliding surface with zero velocity is the origin, the damper appears unlikely to stick. This controller is shown to outperform both a system with all modes critically damped and a system in which all electric fields are set to their maximum values.

1.2. FRICTION MODELLING

Friction has often been modelled by an algebraic equation relating velocity and normal force to friction force. It is well known, however, that friction possesses dynamics associated with varying velocity. A rather complete description of friction modelling and its impact on control appears in reference [10]. It is less well known that there are also dynamics associated with varying the normal force. We assume here that friction dynamics associated with variations in normal force are fast in comparison to those due to velocity fluctuations. Our results to date confirm this assumption.

In this paper, we derive and compare control laws to maximize energy dissipation rate for the first two types of friction model; namely algebraic friction models,

$$f = F_N \mathscr{F}(v), \tag{1}$$

and friction models with velocity dynamics,

$$f = F_N \mathscr{F}(v, z), \qquad \dot{z} = \mathscr{G}(v, z), \tag{2}$$

where the friction force is f, the relative sliding velocity at the friction interface is v and the normal force, F_N, is the control input. Frictional state variables are given by z. $\mathscr{F}$ and $\mathscr{G}$ may be non-linear. Note that in equation (2), friction force can depend, through z, on relative displacement as well as velocity.

The Coulomb model is a simple example of an algebraic friction law satisfying equation (1). In this case, $\mathscr{F} = \mu \, \text{sgn}(v)$, where μ is the coefficient of friction.

As an example of a dynamic friction model, we use a modification of the model proposed by Canudas de Wit and co-workers [13]. This model was designed to reproduce all observed friction phenomena over a wide range of operating conditions. It is given by

$$f = F_N(\sigma_0 z + \sigma_1 \dot{z} + \alpha_2 v),$$

$$\dot{z} = v - \frac{\sigma_0}{g(v)} z|v|, \qquad g(v) = \alpha_0 + \alpha_1 \, e^{-(v/v_0)^2}. \tag{3}$$

Here, z is an internal friction state which represents the average deflection of the asperity junctions. (Asperities are the small peaks on the macroscopically smooth sliding surfaces which compose the actual contact area.) The parameters α_i and v_0 describe the steady state dependence of friction on velocity. The two parameters σ_i control the dynamic dependence of friction on velocity. During sliding, the asperities are deformed elastically and so can store energy. When the sliding direction is reversed, some of this energy is returned to the system. The displacement over which the energy return takes place is given by the value of z just prior to direction reversal.

In the next section, the system dynamic equation is presented and control laws for the two types of friction model are derived. The following section compares these control laws through simulation using the dynamic model of equation (3). The following section presents experimental results for a single damper undergoing forced vibration. The final section contains our conclusions.

2. CONTROLLER DESIGN

We will assume that the system dynamics can be described by a linear model with n degrees of freedom, while friction in the m dampers can be nonlinear. In general, $m < n$. System forcing can be applied as either a disturbance force or a base acceleration. The latter can also be written as an applied force, so that forcing can be denoted generically as F_{ext}:

$$M\ddot{x} + C\dot{x} + Kx + \sum_{i=1}^{m} f_i b_i = F_{ext}. \tag{4}$$

Here, b_i is defined such that $b_i^T x$ is the relative displacement of the ith friction damper and f_i is the friction force in the ith damper.

2.1. ALGEBRAIC FRICTION MODELS

We will assume here that the friction model for an individual damper is of the form

$$f_i = F_{Ni} \mathscr{F}_i(v_i). \tag{5}$$

The function $\mathscr{F}_i(v)$ is memoryless and, to ensure that friction opposes the sliding motion, we assume that it lies in the first and third quadrants. $\mathscr{F}_i(0)$ is allowed to be

multi-valued so as to include the usual models of static friction. Following the Coulomb model, friction force is taken to be linearly dependent on normal force. The sliding velocity v_i at the ith damper is given by $b_i^T \dot{x}$.

In this situation (and similar to references [6, 7]), we can write the total kinetic and potential energy of the system as

$$V = \tfrac{1}{2}(x^T K x + \dot{x}^T M \dot{x}). \tag{6}$$

The rate of change of energy in the system is given by the time derivative of this Lyapunov function,

$$\dot{V} = \dot{x}^T F_{ext} - \dot{x}^T C \dot{x} - \dot{x}^T \left(\sum_{i=1}^{m} F_{Ni} \mathscr{F}_i (b_i^T \dot{x}) b_i \right). \tag{7}$$

Our primary control objective is to maximize the damping provided by the last term in this equation, associated with the friction dampers. At the same time, we wish to ensure global asymptotic stability of the unforced system ($\dot{x} \Rightarrow 0$) under the assumption that the inherent damping term associated with C is negligible. This last assumption is not limiting, as any inherent damping will always augment system stability.

Consequently, we focus on the last term of the preceding equation. Replacing F_{Ni} with u_i yields

$$\dot{V}_d = -\dot{x}^T \left(\sum_{i=1}^{m} u_i \mathscr{F}_i (b_i^T \dot{x}) b_i \right). \tag{8}$$

Since it is assumed that $\mathscr{F}_i$ lies in the first and third quadrants, $\dot{V}_d \leqslant 0$. Assuming that our inputs are bounded, $0 \leqslant u_i \leqslant u_{max}$, the constant application of u_{max} maximizes the instantaneous damping. However, $\dot{V}_d$ is only negative semi-definite and we wish to achieve asymptotic stability of the unforced system. By LaSalle's theorem, the system will converge to the largest invariant set contained in the set satisfying $\dot{V}_d = 0$ [11].

Assuming $F_{ext} = 0$ and $C = 0$, the desired solution $\dot{x} = 0$ is obviously contained in the invariant set. However, the case

$$\dot{x}^T \sum_{i=1}^{m} b_i = 0$$

may be as well. Assuming that the m vectors b_i are independent, this case corresponds to all of the dampers sticking. Since it is expected that there are typically fewer dampers than degrees of freedom ($m < n$), the invariant set associated with constant maximum control effort may include trajectories in which all dampers are sticking and the remaining $n - m$ undamped degrees of freedom contain a constant, but insufficient amount of energy to cause the sticking dampers to slip.

Moreover, each damper should contribute to energy dissipation. If any individual damper sticks (i.e., $\dot{x}^T b_i = 0$ for some i), its energy absorption capacity goes to zero. While this condition does not necessarily affect asymptotic stability, it does reduce the rate at which system energy is dissipated. A damper will remain sticking as long as $\ddot{x}^T b_i = 0$ or

$$b_i^T \ddot{x} = b_i^T M^{-1} \left(F_{ext} - C \dot{x} - K x - \sum_{j=1}^{m} u_j \mathscr{F}_j (b_j^T \dot{x}) b_j \right) = 0. \tag{9}$$

Neglecting the external forcing, this quantity will not remain zero if our friction model is such that $\mathcal{F}_i(0) = 0$. If, however, $\mathcal{F}_i(v)$ is multi-valued at the origin (e.g., Coulomb friction) then it is possible for the damper to remain stuck [12].

The simplest modification of the maximum effort control law which will preclude the sticking condition $\ddot{x}^T b_i = 0$ from being satisfied is the following (in actuality, we need only reduce u_i by the amount necessary to violate the preceding equality):

$$u_i = \begin{cases} u_{max}, & b_i^T \dot{x} \neq 0, \\ 0, & b_i^T \dot{x} = 0. \end{cases} \tag{10}$$

2.2. FRICTION WITH VELOCITY DYNAMICS

We now consider a friction model of the form

$$f = F_N \mathcal{F}, \qquad \dot{\mathcal{F}} = \mathcal{G}(v). \tag{11}$$

We assume that f is stable and that the steady state friction coefficient $\mu_{ss} = f_{ss}(v)/F_N$ lies in the first and third quadrants. Since f now depends on the sliding velocity history, it can no longer be said that instantaneous friction as a function of velocity lies in the first and third quadrants. Friction can now store energy as well as release it into the system.

While friction can now store energy, we remain interested only in the dissipation of energy stored in the mechanical system and so continue to use equation (6) as our energy function. We rewrite equation (8) as

$$\dot{V}_d = -\dot{x}^T \left(\sum_{i=1}^m u_i \mathcal{F}_i b_i \right). \tag{12}$$

To maximize damping with respect to u_i, we arrive at the control law

$$u_i = \begin{cases} u_{max}, & \text{sgn}\,(\mathcal{F}_i \cdot b_i^T \dot{x}) > 0, \\ 0, & \text{otherwise.} \end{cases} \tag{13}$$

This control law maximizes $f_i = u_i \mathcal{F}_i$ when it opposes the direction of relative sliding at the damper as given by sgn $(b_i^T \dot{x})$. Note that this prevents the return of stored frictional energy to the mechanical system. Just as with equation (10), this control law prevents a damper from sticking.

2.3. AVOIDING CHATTER

The proposed control laws are discontinuous and consequently prone to chatter. Chattering occurs in the neighborhood of a switch point (e.g., when a damper velocity is zero) when the switching of a control input, u_i, changes the sign of its acceleration, given by $b_i^T \ddot{x}$ in equation (9). The effect of chattering is to keep the damper velocity near zero rendering the damper largely ineffective.

As we will demonstrate in section 4, the control law can sometimes be modified to avoid chatter when the external forcing is known. In the general case, a simple means of avoiding chatter is the introduction of a boundary layer around the switch point. For example, the control law (10) for an algebraic friction model can be modified to include a piecewise linear boundary layer of thickness ε as follows:

$$u_i = \begin{cases} u_{max}, & |b_i^T \dot{x}| > \varepsilon, \\ (u_{max}/\varepsilon) b_i^T \dot{x}, & |b_i^T \dot{x}| \leqslant \varepsilon. \end{cases} \tag{14}$$

Similarly, control law (13) becomes

$$u_i = \begin{cases} u_{max}, & \text{sgn}\,(\mathscr{F}_i) \cdot b_i^T \dot{x} > \varepsilon, \\ (u_{max}/\varepsilon)\,\text{sgn}\,(\mathscr{F}_i) \cdot b_i^T \dot{x}, & 0 < \text{sgn}\,(\mathscr{F}_i) \cdot b_i^T \dot{x} < \varepsilon, \\ 0, & \text{sgn}\,(\mathscr{F}_i) \cdot b_i^T \dot{x} < 0. \end{cases} \tag{15}$$

In practice, the boundary layer thickness ε should be selected with two criteria in mind. First, since discrete time controllers are most often used, it must be large enough to prevent chatter induced by controller sampling rate and sensor discretization. Second, since we are concerned with unforced stability, ε determines the effective "viscous damping" coefficient during operation within the boundary layer. The latter effect will be made clear in the simulation results which follow.

If stability of the forced system is of interest, the Lyapunov function could be modified to show the relationship between a bound on the external forcing and u_{max}. In this case, the system could be shown to converge to the boundary layer, but Lyapunov stability would not be guaranteed inside the boundary layer.

3. SIMULATION RESULTS

To illustrate the effect of the boundary layer, we consider an example of a damper in which the friction is modelled by equation (3) with the following parameter values taken from reference [13]: $\sigma_0 = 10^5$, $\sigma_1 = 10^3$, $\alpha_0 = 1\cdot0$, $\alpha_1 = 0\cdot5$, $\alpha_2 = 0\cdot2$, $v_0 = 0\cdot1$.

To gain an understanding of the model with these parameters and the effect of the normal force control laws, friction force versus velocity is plotted for the oscillatory velocity $v = 10^{-3} \sin t$ in Figure 1. In this figure, the solid line with circles shows the friction force assuming a constant normal force. In this case, following velocity reversals, the friction force passes through the second and fourth quadrants releasing stored energy into the system. Normal force, as our control input, allows us to scale this plot in the vertical direction. The dashed line of Figure 1 shows friction force versus velocity for a boundary layer thickness of $\varepsilon = 10^{-3}$ and control law (14). The long dash, short dash line shows the
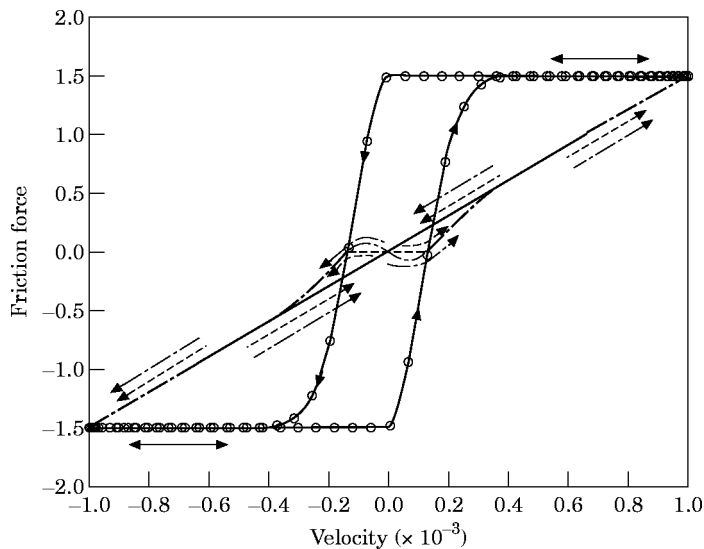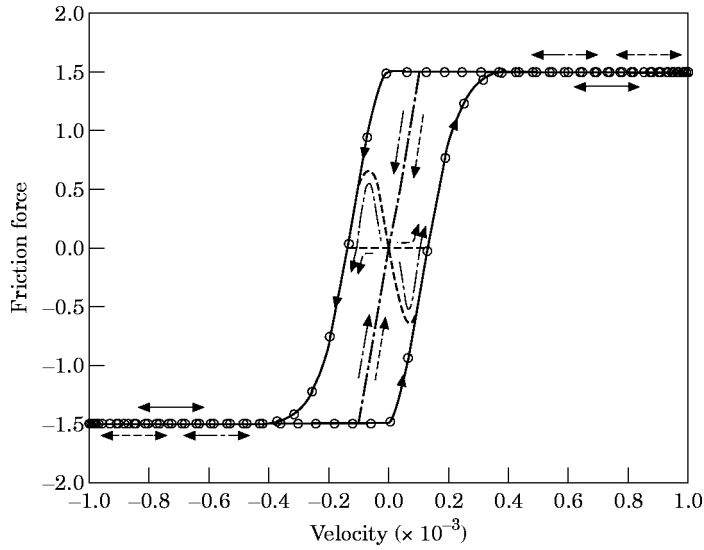

Figure 1. The friction force versus velocity for an oscillatory velocity, $v = 10^{-3} \sin t$. The boundary layer thickness is $\varepsilon = 10^{-3}$. —$\bigcirc$—, $u = u_{max}$; ——, control (14); ———, control (15).

Figure 2. The friction force versus velocity for an oscillatory velocity, $v = 10^{-3} \sin t$. The boundary layer thickness is $\varepsilon = 10^{-4}$. —○—, $u = u_{max}$; ----, control (14); ———, control (15).

result of control law (15) with the same boundary layer thickness. Excursion into the second and fourth quadrants is clearly reduced by either of the control laws. Note, however, that the friction force is also reduced in the first and third quadrants.

The hysteresis loops for $\varepsilon = 10^{-4}$ are depicted in Figure 2. With this very narrow boundary layer, damping is increased in the first and third quadrants. The algebraic control law (14), however, makes larger excursions into the first and third quadrants.

In order to compare control laws (14) and (15) as well as to evaluate the effect of boundary layer thickness, we consider the three-mass system depicted in Figure 3. A friction damper connects the system to its fixed base. This could be considered to be an idealized model of a turbine blade with a damper attached between the root of the blade and the turbine hub.
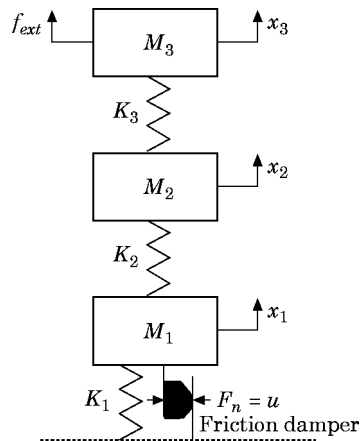

Figure 3. A three-mass idealized model of the turbine blade with a friction damper at the blade root.
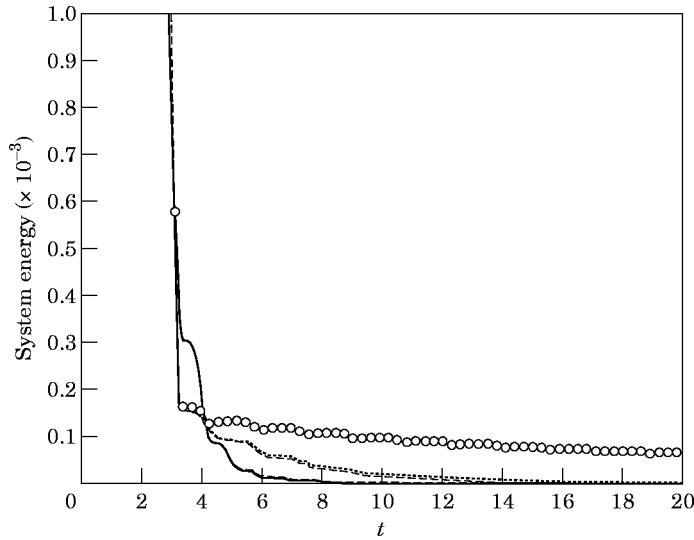
Figure 4. Kinetic plus potential energy in the unforced system. —$\bigcirc$—, $u = u_{max}$; —·—·, control (14), $\varepsilon = 10^{-4}$; $\cdot\cdot\cdot$, control (15), $\varepsilon = 10^{-4}$; ——, control (14), $\varepsilon = 10^{-3}$; ——, control (15), $\varepsilon = 10^{-3}$.

In Figures 4 and 5, the performance of control laws (14) and (15) is compared with the case of constant normal force. The energy in the system is due to initial displacements and velocities; there is no external forcing.

For oscillations involving large displacements and/or velocities, the control laws are nearly equivalent. The difference becomes apparent, however, as the magnitude of the oscillations decreases. For intermediate energy levels ($3 \leqslant t \leqslant 4$), the larger boundary layer is less effective at dissipating energy. For smaller energy levels ($t > 4$), which correspond to small amplitude oscillations of the damper, however, equations (14) and (15) outperform a constant normal force. In fact, for the control law $u = u_{max}$, the damper sticks while masses 2 and 3 continue to oscillate.
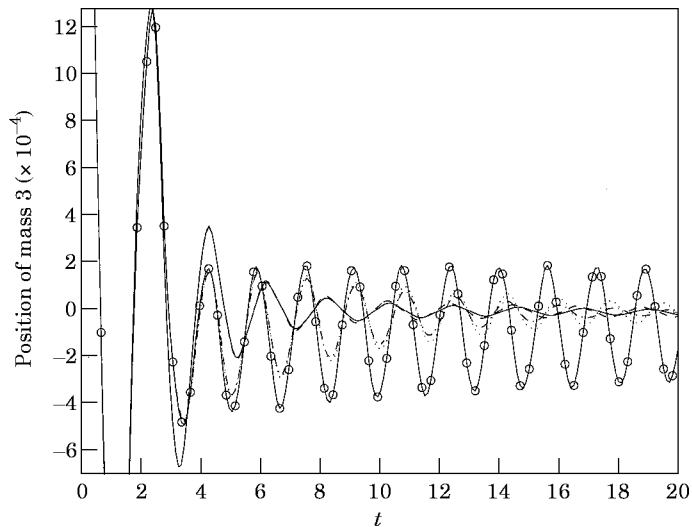

Figure 5. The displacement of mass 3 versus time for the unforced system. —$\bigcirc$—, $u = u_{max}$; —·—·, control (14), $\varepsilon = 10^{-4}$; $\cdot\cdot\cdot$, control (15), $\varepsilon = 10^{-4}$; ——, control (14), $\varepsilon = 10^{-3}$; ——, control (15), $\varepsilon = 10^{-3}$.

As expected, controllers (14) and (15) prevent sticking during small amplitude oscillations. Note that the larger boundary layer is clearly more effective at dissipating system energy in this regime. Examination of the damper displacement trajectories during operation within the boundary layer (not shown) reveals that $\varepsilon = 10^{-4}$ produces an effectively overdamped response while $\varepsilon = 10^{-3}$ achieves critical damping. Ignoring friction velocity dynamics and recalling Figures 1 and 2, one can see that decreasing ε increases the effective viscous damping coefficient within the boundary layer. If this effective coefficient is too large, energy flow from the distal springs and masses into the damper is inhibited.

Clearly, if a boundary layer is implemented, its width should be selected considering both signal noise and desired boundary layer damping. In the experiments described in the next section, a single damper is subjected to sinusoidal forcing. Given that the forcing is known, control law (15) is modified such that chattering is prevented without use of a boundary layer.

4. EXPERIMENTAL RESULTS

To test the efficacy of the proposed control laws experimentally, a double-shear friction fixture was designed, as shown in Figure 6. The friction fixture makes use of a servo-hydraulic materials testing machine (MTM) to provide desired motion trajectories at the friction interface. In this fixture, normal forces are applied to a flat test piece through two cylindrical riders (line contacts). The test piece is attached to MTM's hydraulic actuator which moves it in the vertical direction as indicated by the arrows. The normal forces at the rider/test piece interface are actively controlled using piezo-electric stack actuators (PZTs), which are in series with load cells. The riders are supported in the vertical direction by crossed-roller slide tables. The double-shear design, while averaging the friction forces at the two interfaces, doubles the force sensitivity.

A block diagram of the experimental hardware is shown in Figure 7. The normal force controller consists of a PC with an AD/DA board, load cell, PZT actuators and user-configurable control software. While the range of nominal normal forces that can be applied to the test piece (using the normal force adjustment mechanism) is 0–100 N, the maximum change in normal force produced by the actuator is 25 N. The normal force applied to the test piece was accurate to within 0·15 N.

The MTM's position controller allows user selection of PID gains. Displacement at the friction interfaces is measured with an LVDT which can resolve $\pm 0{\cdot}15$ μm. The transducer
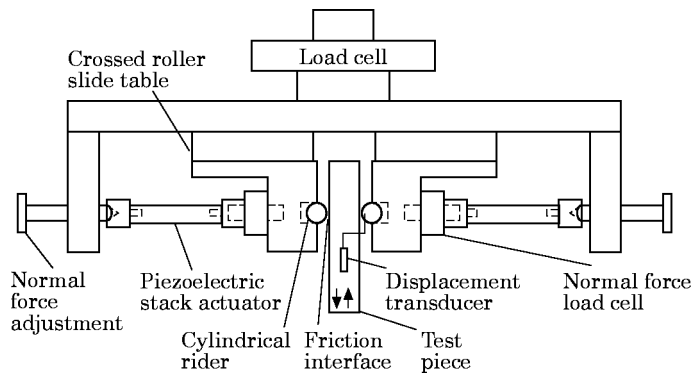

Figure 6. The double-shear friction fixture.

Friction force

Normal force

Displacement

Material testing
machine with
double-shear
friction fixture

A/D

Piezo
stack
actuator

Hydraulic
actuator

Normal
force
controller

Position
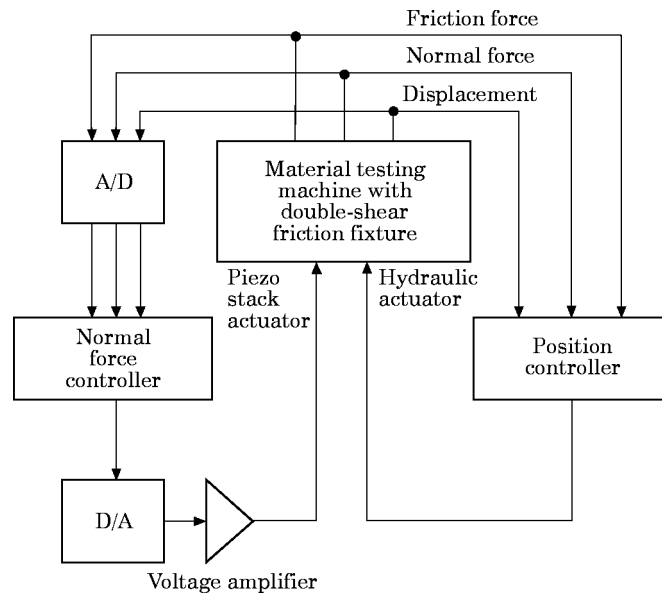controller

D/A

Voltage amplifier

Figure 7. A block diagram of the experimental set-up.

is mounted on the test piece adjacent to the interfaces as shown in Figure 6. The fixture and test piece were designed to be very stiff such that, for the frictional loads applied, the measured displacement and force correspond with the desired accuracy to that of the frictional interface.

The friction force measured using a 10 kN load cell is accurate to within ± 0.25 N. The friction coefficient is obtained by dividing the friction force by twice the normal force.

Since a majority of the applications that employ passive as well as semi-active friction dampers operate in the dry friction regime (i.e., in the absence of lubrication), the experiments detailed in this paper were conducted in this regime. The samples (test piece and riders) used in all experiments were made of A.I.S.I. Grade 1 tool steel which was heat treated and oil quenched to a surface Rockwell hardness of 59C. Both the test piece and the riders were lightly polished with 600 grit paper and washed with acetone between each set of trials (≈ 10).

4.1. EXPERIMENTAL DESIGN

The experiments were designed to compare the dynamic friction control law (13) with the case when the normal force is maintained at its maximum value for forced vibrations of a single-degree-of-freedom system. A block model representation of the experimental fixture appears in Figure 8. In this figure, mass m corresponds to the fixture's test piece which is being forced through the spring and dashpot by a sinusoidal input displacement, $x_{desired}$. The spring and dashpot constants, k_p and k_v, can be adjusted by varying the PD gains of the MTM's position controller while its integral gain is set to zero.

Given that system forcing in these experiments consists of a single frequency, we can compare control laws on the basis of energy dissipated per cycle. In the following sections, we describe the experimental dependence of friction force on forcing amplitude and frequency. These results reveal under what conditions semi-active control will be most beneficial.
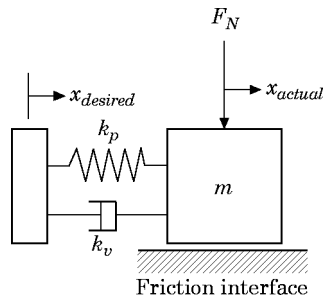
Figure 8. The block model for studying forced vibrations of the experimental fixture.

4.2. FRICTIONAL DEPENDENCE ON FORCING AMPLITUDE

To ascertain the amplitude dependence of friction force, experiments were conducted wherein a sinusoidal frictional displacement was commanded while holding the frequency of oscillation and the normal force at the friction interface constant. The PD gains of the MTM were adjusted such that actual frictional displacement amplitude closely matched the commanded amplitude. A hysteresis plot of friction force versus displacement is shown in Figure 9 for amplitudes of 1, 5, 10, 20 and 50 µm. Each curve in this figure represents an average over 19 cycles. The experiments were conducted at 1 Hz frequency and 50 N normal force.

The area inside an individual hysteresis loop represents the average amount of energy dissipated by the friction damper during one cycle. The shaded regions depicted for amplitudes of 20 and 50 µm represent the amount of stored frictional energy that is returned to the mechanical system following a direction reversal. To maximize energy dissipation, a damper control law should turn off the friction force during the energy return portions of the forcing cycle. This is, in fact, what the proposed control law (13) does.
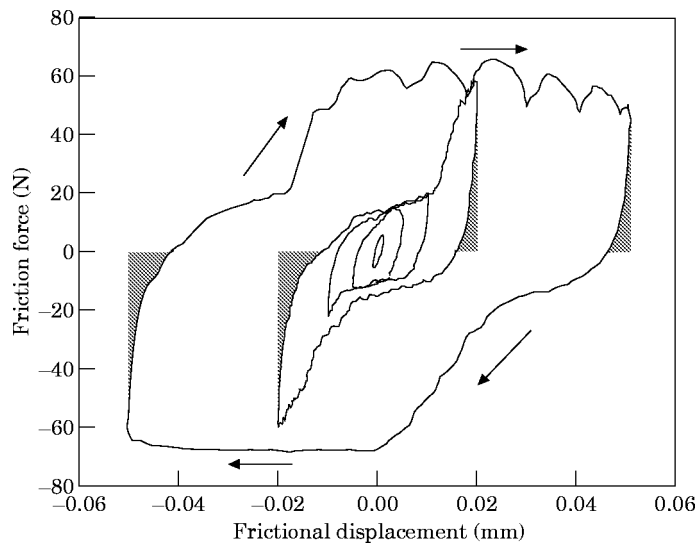

Figure 9. Hysteresis loops showing the amplitude dependence of the friction force at a frequency of 1 Hz and normal force of 50 N. Arrows indicate that loops are traversed clockwise.
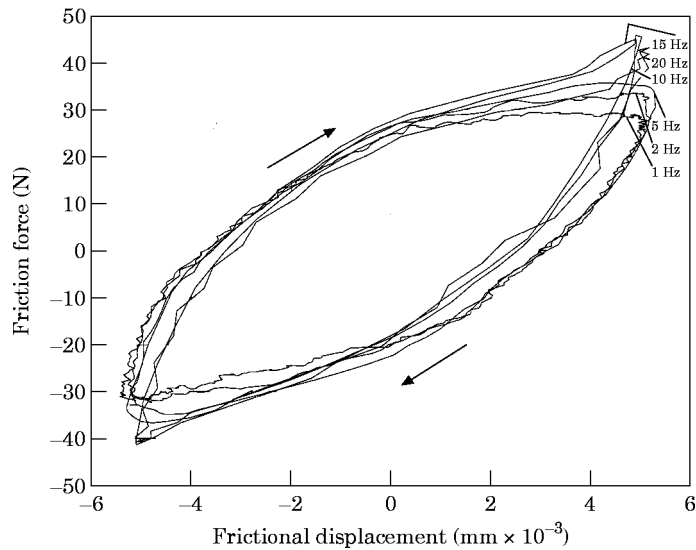
Figure 10. Hysteresis loops showing the frequency dependence of the friction force at an amplitude of 5 μm and a normal force of 50 N. Arrows indicate that loops are traversed clockwise.

Note that as the amplitude of oscillation increases, the amount of stored frictional energy (shaded area) reaches a maximum while the energy dissipated per cycle (area inside the hysteresis loop) continues to grow. This indicates that the potential for increasing energy dissipation through semi-active control (due to velocity dynamics) is largest for small amplitude oscillations—a corroboration of the simulation results.

4.3. FRICTIONAL DEPENDENCE ON FORCING FREQUENCY

To determine the frequency dependence of friction force, experiments were conducted at constant normal force using a sinusoidal friction displacement of fixed amplitude. The tests were repeated for a range of frequencies (1–20 Hz). The resulting hysteresis plots of friction force versus displacement are shown in Figure 10. Each curve in this figure represents an average over 19 cycles. These experiments were performed with a 5 μm amplitude and 50 N normal force.

The experimental results indicate that hysteresis loops remain relatively unchanged with frequency (1–20 Hz range). This conclusion can be extended qualitatively to a forcing frequency of 1 kHz by comparing Figure 10 with Figure 2 in reference [14]. Although different experimental equipment was used to produce these figures, the operating conditions (5 μm amplitude and 50 N normal force) were the same.

From these figures, we can conclude that hysteresis loop shape and size are relatively independent of frequency up to 1 kHz. Consequently, assuming that normal force actuation and frictional response to normal force are fast enough, the potential for increasing energy dissipation through semi-active control is largely dependent on the displacement amplitude.

This frequency range covers most applications of interest. For example, at shroud–shroud interfaces in bladed-disk systems frequencies lie in the range 60 Hz–3 kHz [15–17]. In large space structures, these frequencies are usually in the range of 0·1–5 Hz depending upon the size and stiffness of the structure [2, 3]. Automobile suspension systems in cars and trains can encounter frequencies of oscillation on the order of a few Hertz due to the roughness of roads and guideways respectively [6].

4.4. CONTROL IMPLEMENTATION

Having established that maximum improvement in energy dissipation can be obtained at low amplitudes and that the scope for improvement remains relatively unchanged with frequency, the dynamic controller (13) was implemented at 1 and 10 μm amplitude and 1 Hz frequency of oscillation.

Since the damper was being forced at a single frequency, the control law (13) was modified to preclude any chatter associated with sgn ($\dot{x}$). As a result, a boundary layer as described by equation (15) was not implemented.

The modified controller is described by equation (16), where u is the control input (normal force), F_f is the friction force, and x_{min} and x_{max} are the minimum and maximum displacements. Its operation can be explained as follows. During the half of the cycle when frictional displacement is expected to increase (i.e., from x_{min} to x_{max}), the velocity is assumed to be positive and the control input is based solely on the sign of friction force. Similarly, during the half of the cycle when displacement is expected to decrease (from x_{max} to x_{min}), the velocity is assumed to be negative. Chattering due to control-induced changes in the sign of velocity are thus prevented.

It may also be noted that a normal force pre-load was used which corresponded to 30 N when the controller was "off". With the controller "on", the normal force increased to 50 N:

$$u = \begin{cases} 30, & [(x_{min} \rightarrow x_{max}) \quad \text{AND} \quad (F_f < 0)] \quad \text{OR} \quad [(x_{max} \rightarrow x_{min}) \quad \text{AND} \quad (F_f > 0)], \\ 50, & \text{otherwise.} \end{cases} \quad (16)$$

The controller performance for a displacement amplitude of 2 μm is shown in Figure 11. The two depicted hysteresis loops are averages over four cycles. The loop labeled "Controller OFF" corresponds to a constant normal force of 50 N. The loop labeled "Controller ON" corresponds to equation (16).

Recall that the dynamic friction control law (13) was designed to increase the area of the smaller loop (energy dissipated per cycle) by the shaded areas corresponding to the stored frictional energy. Even though the controller as implemented only reduces the
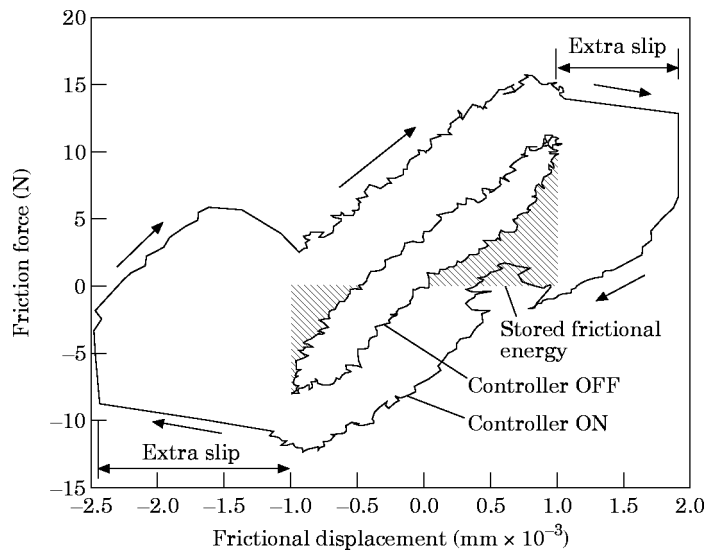

Figure 11. The improvement in energy dissipation due to the dynamic controller.

TABLE 1

Comparison of percentage improvement in energy dissipation

Amplitude of oscillation (μm)	% improvement, velocity dynamics	% improvement, system dynamics	% improvement, total
1	46·41	221·71	268·12
10	14·85	29·03	43·88

normal force to 30 N when turned off (as opposed to 0 N), it increases energy dissipated per cycle by a much larger amount than that predicted by consideration of frictional velocity dynamics.

This is due to the increase in slip amplitude (labelled "extra slip"), which is induced twice per cycle by the sudden drop in normal force following a direction reversal. It can be understood by recalling the equation for damper acceleration, rewritten below for a single damper with $x = x_{actual}$ (using Figure 8, F_{ext} can be expressed in terms of $x_{desired}$ and $\dot{x}_{desired}$):

$$\ddot{x} = (1/m)(F_{ext} - k_v\dot{x} - k_p x - u\mathscr{F}(\dot{x})). \qquad (17)$$

Immediately following a direction reversal, the change in u from 50 to 30 N is sufficient to change the sign of $\ddot{x}$. This causes the damper's effective slip amplitude to increase. Since the controller ignores changes in sgn $(\dot{x})$ during the periods of extra slip, no chattering is induced.

Since the control law was based on an instantaneous optimization, system dynamics, which produce the extra slip, were ignored. From equation (17), the magnitude of extra slip is determined by the system stiffness, damping, effective mass and the friction dynamics. The extra slip was present in all control experiments conducted and its magnitude was found to be relatively independent of the original amplitude of oscillation. The ratio of extra slip to amplitude of oscillation, therefore, increases with decreasing forcing amplitude, thereby increasing the scope for improvement in energy dissipation due to extra slip.

The percentage improvements in energy dissipation for amplitudes of 1 and 10 μm are compared in Table 1. The total percentage improvement is expressed in terms of the improvement expected due to consideration of velocity dynamics and the additional improvement owing to system dynamics. The percentages shown are averages over four experiments (four cycles in each).

5. CONCLUSIONS

We have shown that simple bang–bang control laws, based on an instantaneous maximization of energy dissipation rate, can substantially improve the performance of friction dampers. The beauty of these control designs is that they can be implemented without detailed knowledge of damper friction. Even when friction includes velocity dynamics, at most the sign of the friction force is required.

Whether or not friction velocity dynamics are important depends on the damping application. If the expected amplitude of vibration is large in comparison to the displacement over which friction returns energy to the system (e.g., z), it may be possible to ignore the velocity dynamics altogether. In applications where small amplitude oscillations are expected, our analyses and experiments indicate that a bang–bang control law which accounts for friction dynamics can yield superior performance.

For arbitrary system forcing, use of a boundary layer around the switching points is needed to prevent chattering. Besides requiring excessive control action, chattering associated with velocity zero crossings induces "sticking" of the damper. The boundary layer thickness should be selected taking into account sensor discretization and controller sampling time as well as the desired level of damping within the boundary layer.

If the nature of the system forcing is known, the control law can sometimes be modified to prevent chattering. In the case of sinusoidal forcing, this was demonstrated experimentally with great success.

These experiments also suggest that, for damping applications in which it is feasible to employ more sophisticated sensing and control, significant improvements in performance may be realized by exploitation of the system dynamics. This could be achieved through optimization over a non-zero time period such as the period of forcing.

ACKNOWLEDGMENT

REFERENCES

1. A. SINHA and J. GRIFFIN 1982 *Journal of Aircraft* **20**, 372–376. Friction damping of flutter in gas turbine engine airfoils.
2. R. GRANDHI and G. BHARATRAM 1993 *American Institute of Aeronautics and Astronautics Journal* **31**, 1329–1337. Multiobjective optimization of large-scale structures.
3. M. WHORTON 1995 *Personal Communication*.
4. A. FERRI 1988 *American Institute of Aeronautics and Astronautics, Journal of Spacecraft and Rockets* **25**, 354–360. Modeling and analysis of nonlinear sleeve joints of large space structures.
5. D. KARNOPP, M. CROSBY and R. HARWOOD 1974 *Transactions of the American Society of Mechanical Engineers, Journal of Engineering for Industry* **97**, 619–626. Vibration control using semi-active force generators.
6. J. LANE, A. FERRI and B. HECK 1992 *Friction-Induced Vibration, Chatter, Squeal and Chaos* **DE-Vol. 49**, 165–171. New York: ASME. Vibration control using semi-active frictional damping.
7. N. MCCLAMROCH, H. GAVIN, D. ORTIZ and R. HANSON 1994 *Proceedings of the 33rd Conference on Decision and Control, Lake Buena Vista, FL*, 97–102. Electrorheological dampers and semi-active structural control.
8. K. WANG, Y. KIM and B. SHEA 1994 *Journal of Sound and Vibration* **177**, 227–237. Structural vibration control via electrorheological-fluid-based actuators with adaptive viscous and frictional damping.
9. N. MCCLAMROCH and H. GAVIN 1995 *Proceedings of the 34th Conference on Decision and Control, New Orleans, LA*, 3528–3533. Electrorheological dampers and semi-active structural control.
10. B. ARMSTRONG-HELOUVRY, P. DUPONT and C. CANUDAS DE WIT 1994 *Automatica* **30**, 1083–1138. A survey of models, analysis tools and compensation methods for the control of machines with friction.
11. H. KHALIL 1996 *Nonlinear Systems*. New York: Macmillan; second edition.
12. P. DUPONT 1993 *International Journal of Robotics Research* **12**, 164–179. The effect of friction on the forward dynamics problem.
13. C. CANUDAS DE WIT, H. OLSSON, K. ASTROM and P. LISCHINSKY 1995 *IEEE Transactions on Automatic Control* **40**, 419–425. A new model for control of systems with friction.
14. K. SANLITURK, A. STANBRIDGE and D. EWINS 1995 *American Society of Mechanical Engineers, 15th Biennial Conference on Mechanical Vibration and Noise* **DE-Vol. 84-2**, 1377–1382. Friction dampers: measurement, modelling, and application to blade vibration control.
15. D. EWINS and Z. HAN 1984 *Journal of Vibration, Acoustics, Stress, and Reliability in Design* **106**, 211–217. Resonant vibration levels of a mistuned bladed disk.

16. D. Ewins and M. Imregun 1984 *Journal of Vibration, Acoustics, Stress, and Reliability in Design* **106**, 175–180. Vibration modes of packeted bladed disks.
17. A. Srinivasan and D. Cutts 1984 *Journal of Vibration, Acoustics, Stress, and Reliability in Design* **106**, 189–197. Measurement of relative vibratory motion at the shroud interfaces of a fan.